JOURNAL OF AIRCRAFT
Vol. 43, No. 6, November–December 2006

Optimal Scheduling of Control Surfaces on Flexible Wings to Reduce Induced Drag

Raymond M. Kolonay*
U.S. Air Force Research Laboratory, Wright-Patterson Air Force Base, Ohio 45433
and
Franklin E. Eastep†
University of Dayton, Dayton, Ohio 45469

DOI: 10.2514/1.14604

Induced drag on flexible wings is reduced at off-design cruise conditions with simulated active conformal control surface deflections. An inverse optimization technique is used to manipulate the spanwise distribution of load. The method is demonstrated on two cases, a simple rectangular wing with a beam model and a fighter wing with a fully built-up finite element structural model. The control surfaces are deflected to redistribute the lift on the wing while maintaining a two degrees of freedom (lift and pitch) flexible trimmed flight condition. Iteratively optimizing an approximate problem eliminates the need for the trimmed angle of attack and the elevator deflections to participate in the design optimization as free variables. Only the control surface deflections are used to match the desired elliptic load distribution, which in turn is shown to produce the minimum induced drag according to calculations by a Trefftz-plane technique. The automated structural optimization system program is used for creating a complex structural model, a realistic linear aerodynamic prediction technique, and a free flying trim analysis.

Nomenclature

a	=	semiminor axis of desired elliptical lift distribution
b	=	semimajor axis of desired elliptical lift distribution
C_{DI}	=	coefficient of induced drag
$F(\beta_i, \alpha, \delta_e)$	=	objective Function
F_n^{desired}	=	desired force-per-unit span at the nth span location
$F_n^{\mathrm{calculated}}$, F_i	=	calculated force-per-unit span at the nth, ith spanwise strip
$g(\beta_i, \alpha, \delta_e)$	=	constraint
$\bar{g}$	=	constraint allowable
M	=	Mach number
ns	=	number of spanwise strips on the wing planform
q	=	dynamic pressure
S_{total}	=	total planform area
V_0	=	freestream velocity
w_i	=	total downwash at y_i produced by all trailing vortices
y_i, y_n	=	spanwise coordinate at the midpoint of the ith/n th strip
y_k	=	spanwise coordinate of the right edge of the k strip
α	=	angle of attack of wing
$\alpha_{\mathrm{induced}}$	=	induced angle of attack for a given spanwise strip/panel
α_{trim}	=	trimmed angle of attack of wing
β_i	=	ith design variable: control surface deflection angle for the ith control surface
β^L, β^U	=	upper and lower bounds on the design variables
Δw_i	=	incremental downwash at a point y_i produced by a single trailing vortex at y_k
Δy_i	=	span width of the ith strip
$\delta_{e_{\mathrm{trim}}}$	=	trimmed elevator/horizontal tail deflection
δ_e	=	angle of attack of elevator/horizontal tail
ρ_∞	=	free steam density of air
$\Gamma(y)$	=	span circulation distribution
Γ_k	=	circulation at the kth spanwise strip $= F_1/\rho_\infty V_0$

Introduction

THE wing of a flight vehicle is generally tapered and twisted (jig shape) in the spanwise direction to approximate an elliptic aerodynamic lift distribution at a given flight condition, typically a cruise condition. This results in a reduction of the induced drag at that given design condition. Unfortunately, flexibility and operating at other flight conditions causes deviation from the elliptic spanwise lift distribution and results in an increase of induced drag. To return to the desired lift distribution at any flight condition including structural flexibility effects, trailing-edge control surfaces are deflected in a manner to obtain the elliptic spanwise lift distribution resulting in a reduction of induced drag.

Two approaches have emerged in the literature concerning the design of lifting surfaces while considering induced drag. The first approach computes the induced drag directly and minimizes this, whereas the second method assumes that an elliptical spanwise distribution produces a configuration that has minimum induced drag. Weisshaar et el. [1] give a comprehensible historical review of the design of lifting surfaces considering the reduction of induced drag as an objective. In addition, they proceed to develop an optimization technique that obtains the optimal structural planform configuration along with wing laminate designs and control surface deflections that minimize induced drag by producing a spanwise elliptic load distribution. This technique employs a cantilevered coupled beam model that represents the structural behavior and strip theory for the aerodynamics. Weisshaar et al. [1] conclude that wing induced drag could be reduced with either passive wing aeroelastic tailoring, control surface settings, or a combination of both. As an example of computing the induced drag approach, Raveh and Levy [2] use trailing-edge control surfaces to minimize induced drag while

Presented as Paper 4362 at the 10th AIAA/ISSMO Multidisciplinary Analysis and Optimization Conference, Albany, New York, 1–4 September 2004; received 15 November 2004; revision received 28 December 2005; accepted for publication 28 January 2006.

*Senior Research Aerospace Engineer, Structures Division, 2130 Eighth Street; Raymond.kolonay@wpafb.af.mil. Associate Fellow AIAA.

†Emeritus Professor, Mechanical and Aerospace Engineering, College Park Drive; franklin.eastep@wpafb.af.mil. Fellow AIAA.

using angle of attack to maintain trimmed flight. They formulate the problem as a linear programming problem and compute the necessary sensitivities by finite differences. Raveh and Levy [2] compute the aerodynamic surface pressures using an Euler solver whereas the structural model is represented by generalized coordinates (generalized mass, generalized stiffness, and mode shapes). The goal of their work is to develop an efficient CFD-based algorithm for the determination of the aeroelastic response of a wing with multiple deflected control surfaces that could be used in the design of highly flexible wings. Raveh and Levy [2] calculated that the minimization of the computed induced drag by deflecting multiple control surfaces results in an elliptic spanwise lift distribution. Kuzmina et al. [3] also compute the induced drag and minimize it by deflecting trailing-edge control surfaces while maintaining a trimmed flight condition for lift and pitch degrees of freedom. Kuzmina et al. [3] use a doublet lattice method for representation of the aerodynamics and a set of generalized coordinates and appropriate mode shapes to represent the structural characteristics of the flight vehicle. They compute induced drag as a function of circulation on the wing and the downwashes governed by a vortex sheet exiting from the trailing edge of the wing. With the computed circulation and downwashes, the coefficient of drag can be found as a quadratic function of the generalized coordinates and can be reduced by selecting the appropriate control surface settings. Finally, Eller and Heinze [4] computed induced drag associated with control surface deflections and compared the calculated values to experimental results.

In the current study, the aircraft wing structure is assumed to be a complex assemblage of interconnected elements composed of both metallic and composite materials. To capture the physics of the structural response at an appropriate level of accuracy the finite element method is employed to model the aircraft structure. The external aerodynamic loads distribution in both the chord and span direction are predicted using the USSAERO [5] paneling method. In this research, both the structural and aerodynamic representations remain in physical coordinates. Generalized coordinates are not employed. The automated structural optimization system (ASTROS) [5] is used for modeling the structure, the steady aerodynamic loads, and carrying out the lift and pitch trim analysis of a free flying flexible air vehicle.

Two wing models are selected for this investigation. The first model, referred to as the Goland wing [6], has a "beam-rod" structural model. The second model considered is a built-up model typical of a fighter-type aircraft [7]. Both models have 20 discrete control surfaces along the trailing edge of each aerodynamic model. The aerodynamic effects of gaps between each of the discrete surfaces are ignored to simulate conformal control surfaces to ensure profile drag is minimal by eliminating edge effects [8].

R. T. Jones [9] has demonstrated that wings having an elliptical spanwise lift distribution ensures minimum induced drag. Therefore, in the present study, the control surfaces are scheduled to obtain an elliptical spanwise load distribution. It is worth noting that the methodology developed in this work is general and can be used to obtain any desired distribution, not just elliptical. In addition, as demonstrated by Munk [10], induced drag is independent of the distribution of lift in the chordwise direction. For the current study, induced drag calculations are carried out considering the "Trefftz-plane" [11] downstream from the trailing edge. The wing is held at a trimmed (for lift and pitch) level flight condition using the angle of attack and elevator, whereas the control surfaces are used only to obtain the desired elliptical spanwise pressure distribution.

Optimization Problem Statement

The problem is posed as an inverse optimization problem similar to the development in [12]. Given a desired response (load distribution), a set of design variables (control surfaces) are modified to obtain the desired response. The objective is to minimize the error between the desired response and the actual response. The inverse problem can be stated in the following optimization form:

$$\text{Minimize}: F(\beta_i, \alpha, \delta_e)$$

subject to constraints

$$g(\beta_i, \alpha, \delta_e) = \bar{g} \qquad \beta^L < \beta_i < \beta^U \tag{1}$$

The objective is defined as the sum of the square of the errors between the desired response at each spanwise strip on the wing and the actual response. This can be written as

$$F(\beta_i, \alpha, \delta_e) = \sum_{n=1}^{\text{ns}} (F_n^{\text{desired}} - F_n^{\text{calculated}})^2 \tag{2}$$

The F_n depend on the control surface deflections, the angle of attack, and the elevator deflection. The equality constraint $g(\beta, \alpha, \delta_e) = \bar{g}$ represents the fact that the lifting surface must remain in a trim state. For the current work, symmetric trim for lift and pitch is considered.

Solution of the Optimization Problem

A gradient-based optimization solution of Eq. (1) is used. In addition, an approximate problem technique is employed. This entails the construction of approximate functions for the objective, constraints, and their respective gradients before passing the problem to the optimization routine. This creates the need for an outer loop iteration which is required to determine convergence of the exact problem. This approach reduces the number of exact engineering analyses that need to be made. With this approach, the constraint in Eq. (1) that represents maintaining trimmed flight are not submitted to the optimization routine. Instead, α and δ_e are assumed constant during a given approximate problem and are only varied when an exact analysis is performed. That is, only α and δ_e are used to trim the configuration. The β_i are varied during the approximate optimization to obtain the desired load distribution but are assumed constant during the trim analysis. With these assumptions, Eq. (1) is written as

$$\text{Minimize}: F(\beta_i)$$

subject to constraints

$$\beta^L < \beta_i < \beta^U \tag{3}$$

Equation (3) indicates that the objective function is now only a function of the β_i and the constraint $g(\beta_i, \alpha, \delta_e)$ no longer appears in the approximate problem submitted to the optimization routine even though it depends on β_i. This is justified by the fact that the sensitivity of $g(\beta_i, \alpha, \delta_e)$ to β_i for the cases studied are one to two orders of magnitude smaller than the sensitivities due to α and δ_e (see Tables 1 and 2). Hence, for this work, the constraint is not explicitly supplied to the optimization routine; it is enforced by performing a trim analysis after an optimum of the approximate problem is reached. Therefore, the only constraints supplied to the optimization routine are the side constraints ($\beta^L < \beta_i < \beta^U$).

Specification of the Objective Function

The desired response F^{desired} is represented by any analytical function. For this work an elliptical shape of the form $(a)(1 - y_i^2/b^2)^{1/2}$ is chosen for the desired load distribution. The wing semispan is selected as b, and a is $F_1^{\text{calculated}}$ (total force at strip 1, that is the strip at the wing root) for the given trim condition. Figure 1 illustrates the calculated and desired F_n along with the definitions of a and b.

The definition of a implies it is dependent on both β, α, and δ_e, and varies between approximate optimization problems, but is considered constant during an approximate optimization. With this assumption for F^{desired}, Eq. (2) becomes

$$F(\beta) = \sum_{n=1}^{\text{ns}} \left[(a)\left(1 - \frac{y_i^2}{b^2}\right)^{1/2} - F_n^{\text{calculated}} \right]^2 \tag{4}$$

Table 1 Goland wing flexible stability derivatives $M = 0.7$, $q = 322$ psf

Parameter	Label	Units	Lift	Pitching moment
Angle of attack	ALPHA	1/rad	7.4909	−2.4657
Control surface	ELEV	1/rad	1.7096	−1.7215
Pitch rate	QRATE	S/rad	16.2688	−10.7745
Control surface	CS1	1/rad	−0.0026	0.1026
Control surface	CS2	1/RAD	−0.0032	0.0992
Control surface	CS3	1/rad	−0.0014	0.0922
Control surface	CS4	1/rad	0.006	0.0795
Control surface	CS5	1/rad	0.0255	0.0546
Control surface	CS6	1/rad	0.0757	−0.0007
Control surface	CS7	1/rad	0.2253	−0.1547
Control surface	CS8	1/rad	0.2089	−0.143
Control surface	CS9	1/rad	0.1903	−0.1287
Control surface	CS10	1/rad	0.1755	−0.118
Control surface	CS11	1/rad	0.1634	−0.1099
Control surface	CS12	1/rad	0.1532	−0.1035
Control surface	CS13	1/rad	0.1439	−0.098
Control surface	CS14	1/rad	0.1353	−0.0932
Control surface	CS15	1/rad	0.1266	−0.0886
Control surface	CS16	1/rad	0.1175	−0.0838
Control surface	CS17	1/rad	0.1072	−0.0784
Control surface	CS18	1/rad	0.0947	−0.0715
Control surface	CS19	1/rad	0.0781	−0.0615
Control surface	CS20	1/rad	0.0509	−0.0423

Table 2 Fighter wing flexible stability derivatives $M = 0.7$, $q = 8.5$ psi

PARAMETER	Label	Units	Lift	Pitching moment
Angle of attack	ALPHA	1/rad	9.7215	−2.5381
Control surface	ELEV	1/rad	1.5285	−1.2559
Pitch rate	QRATE	S/rad	7.6747	−3.4782
Control surface	CS1	1/rad	0.0563	−0.0198
Control surface	CS2	1/rad	0.4021	−0.3066
Control surface	CS3	1/rad	−0.103	0.084
Control surface	CS4	1/rad	−0.1676	0.1352
Control surface	CS5	1/rad	−0.1747	0.1232
Control surface	CS6	1/rad	−0.5126	0.3694
Control surface	CS7	1/rad	−0.2719	0.1662
Control surface	CS8	1/rad	−0.1952	0.0617
Control surface	CS9	1/rad	0.0481	−0.1387
Control surface	CS10	1/rad	−0.1082	−0.043
Control surface	CS11	1/rad	−0.17	−0.0101
Control surface	CS12	1/rad	−0.2201	0.0235
Control surface	CS13	1/rad	−0.1891	0.0124
Control surface	CS14	1/rad	−0.1827	0.0322
Control surface	CS15	1/rad	−0.3738	0.093
Control surface	CS16	1/rad	−0.0912	0.0161
Control surface	CS17	1/rad	−0.3452	0.1063
Control surface	CS18	1/rad	−0.2236	0.0731
Control surface	CS19	1/rad	−0.0379	0.0348
Control surface	CS20	1/rad	−0.2092	0.0758

It is important to note that the elliptical shape was chosen as an example. The method is general and any shape or desired distribution can be specified. With the elliptical shape chosen for the desired shape, the gradient of the objective function with respect to the design variables is computed as follows:

$$\frac{\partial F}{\partial \beta_i} = \sum_{n=1}^{\text{ns}} 2\left[a\left(1-\frac{y_n^2}{b^2}\right) - F_n^{\text{calculated}}\right] \times \left[\frac{\partial a}{\partial \beta_i}\left(1-\frac{y_n^2}{b^2}\right)^{1/2} - \frac{\partial}{\partial \beta_i} F_n^{\text{calculated}}\right] \tag{5}$$

Inspection of Eq. (5) reveals that the calculation of $\partial a/\partial \beta_i$ and $(\partial a/\partial \beta_i)F_n^{\text{calculated}}$ are required. The change in the minor axis of the ellipse with respect to β_i is $\partial a/\partial \beta_i$. As described, a is assumed to be $F_1^{\text{calculated}}$ and thus $\partial a/\partial \beta_i = (\partial a/\partial \beta_i)F_1^{\text{calculated}}$. Equation (5) is now restated as

$$\frac{\partial F}{\partial \beta_i} = \sum_{n=1}^{\text{ns}} 2\left[a\left(1-\frac{y_n^2}{b^2}\right) - F_n^{\text{calculated}}\right] \times \left[\frac{\partial}{\partial \beta_i} F_1^{\text{calculated}}\left(1-\frac{y_n^2}{b^2}\right)^{1/2} - \frac{\partial}{\partial \beta_i} F_n^{\text{calculated}}\right] \tag{6}$$

For this work only, linear aerodynamics are used. This results in $(\partial a/\partial \beta_i)F_n^{\text{calculated}}$ being constants throughout the optimization process and are required to be calculated only once for a given Mach number, dynamic pressure, and set of structural parameters. For the present study, $(\partial a/\partial \beta_i)F_n^{\text{calculated}}$ are determined by finite difference making the sensitivities semi-analytic.

Trefftz-Plane Induced Drag Calculations

The preceding section describes an optimization procedure to determine trailing-edge control surface settings to insure the span aerodynamics force distribution is a specified shape (elliptical in this

case) while the aircraft is in a trimmed flight condition. The aerodynamic pressure distribution in both the chord and span directions are calculated with the USSAERO [5] paneling method. The aerodynamic force-per-unit span is determined by summing the chord aerodynamic forces over each aerodynamic strip (see Fig. 3). To track the induced drag for each iteration shown in Fig. 4, the following calculation procedure for induced drag is used.

Munk [10] proved from his displacement theorem that it is immaterial for determining the magnitude of induced drag whether the circulation distribution in the chord direction is caused by wing planform, wing twist, or by camber of the wing. That is, the entire induced drag may be calculated without taking into consideration the transverse vortices, thus the calculation method is greatly simplified by using only the longitudinal vortices. With the Munk displacement theorem, one can calculate induced drag by using a Trefftz-plane located far downstream from the lifting surface. Figure 2 illustrates the span circulation distribution and the trailing vortices as viewed from the Trefftz-plane. The strength of the trailing vortices $\Gamma_k - \Gamma_{k+1}$ can be determined from the Kutta–Joukowski equation relating the span aerodynamic force to the strength of the bound or transverse vortex as $F_i = \rho_\infty V_0 \Gamma_i$.

The trailing vortices appear to be line vortices of strength $\Gamma_k - \Gamma_{k+1}$. The span loading is assumed to be symmetric and only span points on the right wing need be considered. The increment of downwash at a point at the center of a strip caused by a trailing line vortex of strength $\Gamma_k - \Gamma_{k+1}$ located at the right point of a different strip is

$$\Delta w_i = \left(\frac{\Gamma_k - \Gamma_{k+1}}{4\pi}\right)\left[\frac{1}{y_i - y_k} - \frac{1}{y_i + y_k}\right] \qquad \begin{matrix} i = 1, \ldots, N \\ k = 1, \ldots, N \end{matrix} \qquad y_i \neq y_k \tag{7}$$

where N is the total number of strips on the right wing. The total downwash produced by all the trailing vortices is then:

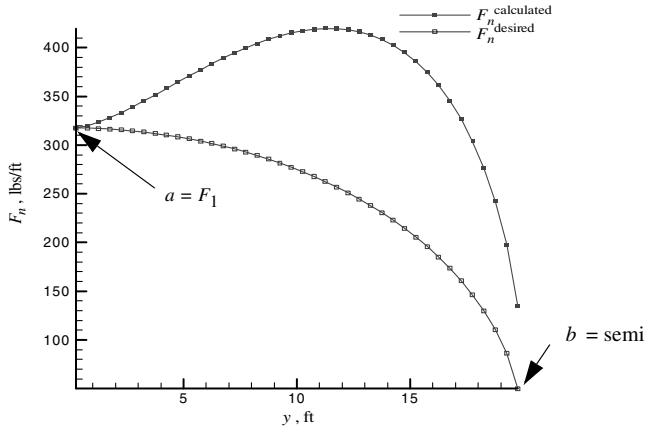

Fig. 1 Calculated and desired force-per-unit span vs span.

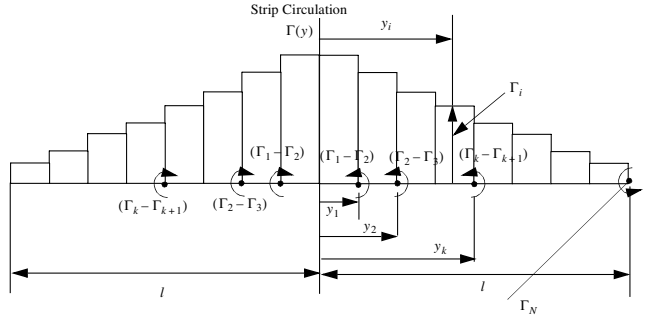

Fig. 2 Wing circulation distribution and trailing vortices viewed from Trefftz-plane.

$$w_i = \left(\frac{1}{4\pi}\right)\sum_{k=1}^{N}(\Gamma_k - \Gamma_{k+1})\left[\frac{1}{y_i - y_k} - \frac{1}{y_i + y_k}\right] \tag{8}$$
$$i = 1, \ldots, N \qquad y_i \neq y_k$$

It is important to note that in Eq. (8) when $k = N$, $\Gamma_N - \Gamma_{N+1} = \Gamma_N$. Expressed in matrix form, Eq. (8) becomes

$$\{w\} = \frac{1}{4\pi}[AIC]\{\bar{\Gamma}\} \tag{9}$$

and the induced angle of attack is

$$\{\alpha_{\text{induced}}\} = -\frac{1}{V_0}\{w\} \tag{10}$$

with V_0 representing the freestream velocity. The total induced drag D_{induced} and the coefficient of drag can now be expressed as

$$D_{\text{induced}} = \lfloor F \Delta y \rfloor \{\alpha_{\text{induced}}\} \qquad C_{\text{DI}} = \frac{D_{\text{induced}}}{qS_{\text{total}}} \tag{11}$$

Hence, D_{induced} is expressed solely in terms of F_i and the spanwise coordinates. The linear aerodynamic prediction technique within ASTROS is used to determine the respective F_i.

Results

Two cases were considered to demonstrate the method. The planforms used are the Goland wing and a fighter wing. Both cases are evaluated for trimmed level flight at $M = 0.7$.

Goland Wing

Figure 3 shows the planform and box pattern for the Goland wing developed in [2], along with an additional horizontal tail. The structural model is a simple beam located 1.98 ft from the leading edge of the wing. It is important to note that the horizontal tail has no structural model associated with it. It is only modeled aerodynamically and its resultant loads are applied to the support point via a rigid transformation of the resulting forces and moments.

Twenty equally sized (20% chord length, 12 in. width) control surfaces are located at the trailing edge of the planform. For a Mach

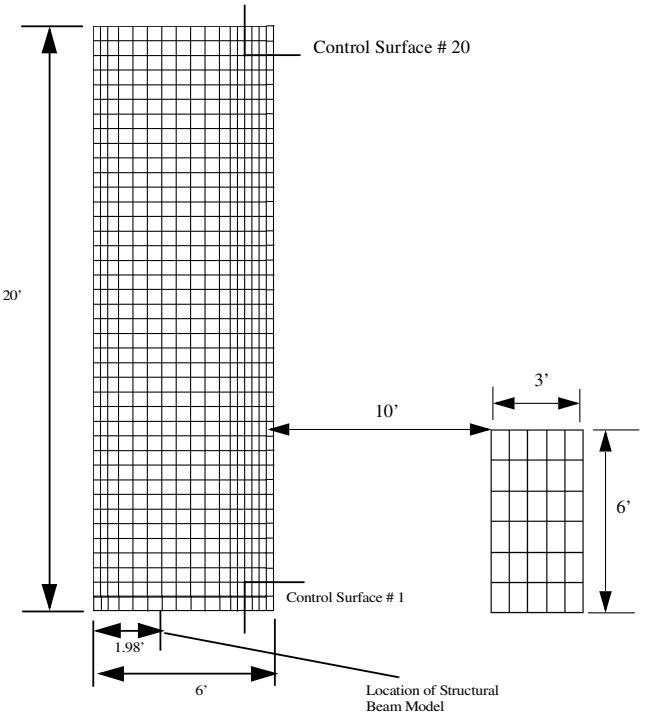

Fig. 3 Goland wing aerodynamic and structural model.

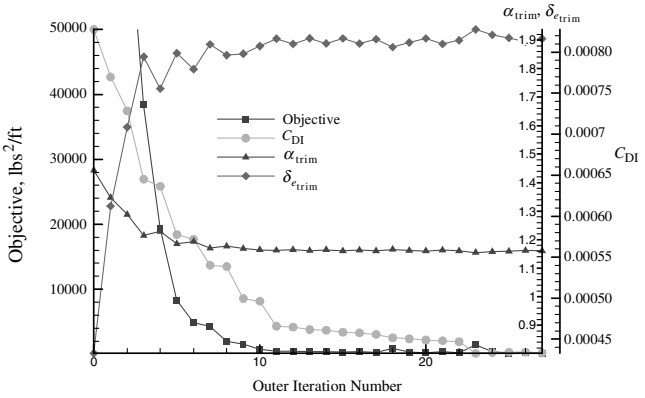

Fig. 4 Goland wing objective, C_{DI}, α_{trim}, $\delta_{e_{\text{trim}}}$ vs iteration $M = 0.7$, $q = 322$ psf.

number of 0.70, a dynamic pressure $q = 322$ psf, and trimmed level flight at a load factor of one times gravity, the scheduling of the control surfaces are determined to create a spanwise elliptical load distribution. Table 1 is a listing of the flexible stability derivatives for the configuration at the specified flight conditions. This table indicates that the sensitivities of trim conditions of lift and pitch with respect to the control surface deflections are small (one to two orders of magnitude smaller) compared with the senstivities of ALPHA, ELEV, and QRATE. This information is used to justify not explicitly supplying the trim constraint g to optimizer. The trim constraint is enforced by performing a trim analysis after an optimum of the approximate problem is reached. Figure 4 contains the objective function, trimmed angle of attack, trimmed elevator deflection, and the coefficient of induced drag vs the iteration history of the exact optimization problem (as opposed to the approximate problem submitted to the optimizer). This figure shows several things. First, the objective function exhibits convergence. Second, the induced drag decreases as the objective decreases. This indicates that movement toward an elliptical spanwise distribution does reduce the induced drag computed by the Trefftz-plane [11] theory. Finally, Fig. 4 shows the variation of the angle of attack and elevator setting required to maintain a trimmed flight condition throughout the exact or outer loop optimization problem. Figure 5 depicts the initial and final stripwise forces F_n vs span. Both the desired values and the actual calculated values are represented. Here, one can see that the initial $F_n^{\text{calculated}}$ is quite different from the desired elliptical distribution. After the optimization, the F_n^{desired} and $F_n^{\text{calculated}}$ are essentially identical. Also, it can be observed that the trimmed angle of attack and trimmed angle of the elevator are changing as the optimization is progressing. This is seen in Fig. 4 but also shows up in Fig. 5 by the fact that F_1^{initial} and F_1^{final} have different values. Figure 6 illustrates the final pressure distribution and the final control surface

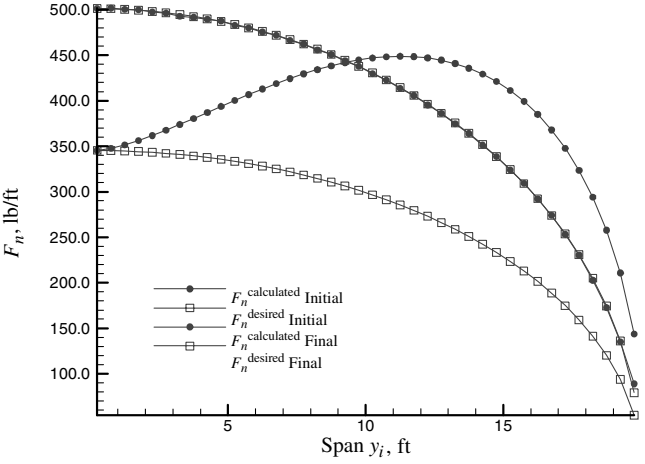

Fig. 5 Goland wing F_n vs span, $M = 0.7$, $q = 322$ psf.

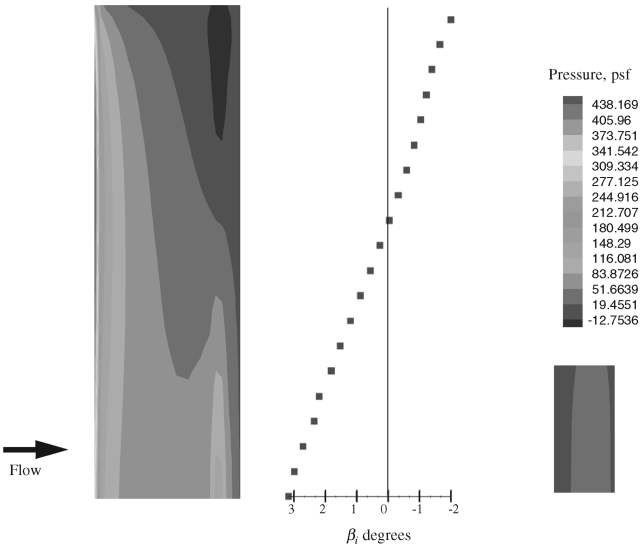

Fig. 6 Goland wing pressure and β_i for final design, $M = 0.7$, $q = 322$ psf.

deflection values $\beta_{i\text{final}}$. This figure shows the impact of the control surface deflections on the wing pressures. It can also been seen in Fig. 6 that the control surface deflection pattern is relatively smooth when moving from inboard span locations to outboard span locations, and the $\beta_{i\text{final}}$ crossover from a positive deflection (downward) to a negative deflection (upward) near the midspan.

Fighter Wing

The fighter wing model used is a modified version found in [7]. Here, the wing structure is terminated at the wing root (no carry-through attachment). In addition, 20 trailing-edge control surfaces are added to the aerodynamic model along with the horizontal tail. Once again, as with the previous case, there is no structural representation for the horizontal tail but it is included to trim the vehicle. The wing structural model uses isoparametric quadrilateral/triangular membranes for the skins, rod elements for the post and spar caps, along with shear elements for the ribs and spars. Figure 7 shows the structural and aerodynamic model used for the current study. For a Mach number of 0.7 and a dynamic pressure of 8.5 psi, a baseline aeroelastic trim analysis (1 g level flight) is performed using the wing angle of attack and the horizontal tail to trim the aircraft for lift and pitch. The unrealistically high dynamic pressure is chosen to exaggerate the differences between the flexible spanwise loads and the desired elliptical distribution. Table 2 is a listing of the flexible stability derivatives for the configuration at the specified flight conditions. As for the Goland wing example, this table indicates that

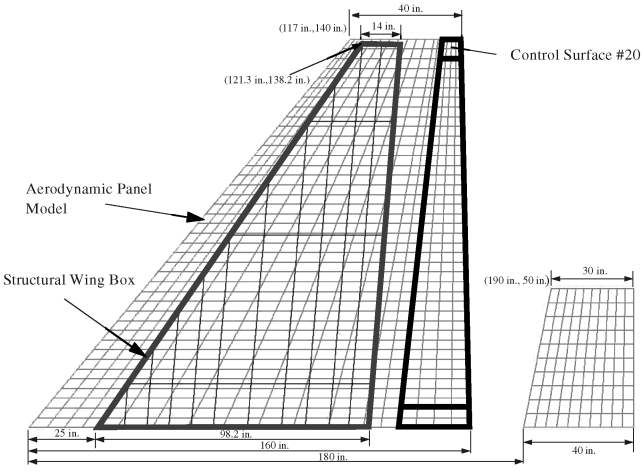

Fig. 7 Fighter wing aerodynamic and structural model.

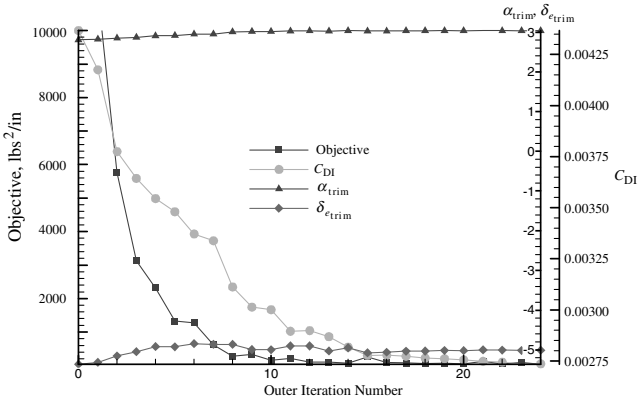

Fig. 8 Fighter wing objective, C_{DI}, α_{trim}, $\delta_{e_{\text{trim}}}$ vs iteration $M = 0.7$, $q = 8.5$ psi.

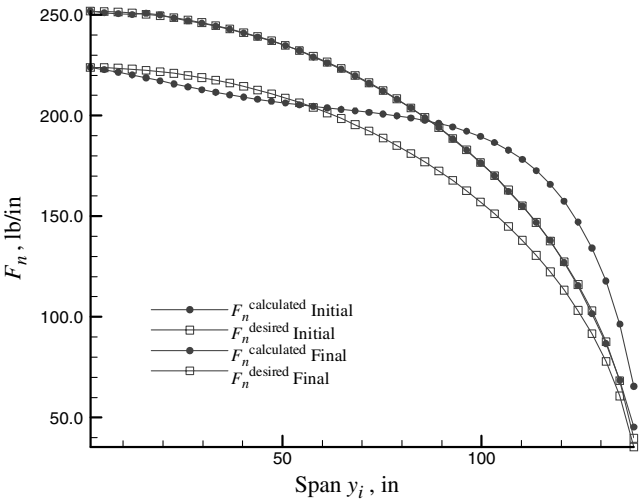

Fig. 9 Fighter wing F_n vs span, $M = 0.7$, $q = 8.5$ psi.

the sensitivities of trim conditions of lift and pitch with respect to the control surface deflections are small (one to two orders of magnitude smaller) compared with the sensitivities of ALPHA, ELEV, and QRATE. Once again, to reduce computational cost, the trim constraint is not explicitly supplied to the optimizer. Figure 8 is a plot of the objective function vs iteration of the exact optimization problem and indicates convergence to an optimal solution. Figure 9 shows a plot of F_n vs span for the baseline case and the final optimized solution. The open square symbols represent the initial desired elliptical distribution (F_n^{desired} initial) and the closed square symbols indicate the initial calculated distribution ($F_n^{\text{calculated}}$ initial). Figure 9 also contains the final optimized solution, both the desired distribution final and actual calculated distribution final. A few observations are made concerning Fig. 9: first, the optimization does well at matching the calculated values with the desired elliptical shape. Second, it can be seen that the root value F_1 of the desired distribution changes during the optimization process. For this case, it moves from approximately 230 lb/in to about 250 lb/in. This is due to the fact that the vehicle must remain trimmed throughout the process. Recall that only α and δ_e are being used to trim the aircraft. The control surfaces are used only to obtain the appropriate shape of the spanwise load. In obtaining the desired shape, the control surfaces obviously have an impact on the lift generated on the wing. The surfaces may increase or decrease the lift overall depending on their deflections. In this case, they decrease the lift which requires α_{trim} to increase and $\delta_{e_{\text{trim}}}$ to increase to maintain a trimmed condition. This results in a larger F_1 value. Finally, Fig. 10 contains a contour plot of the final aeroelastic trimmed pressures (optimized control surface deflections) along with the final control surface deflections for all 20 control surfaces. This figure illustrates that the first 15

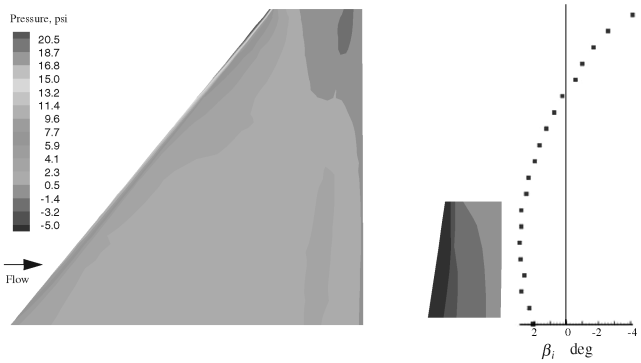

Fig. 10 Fighter wing pressure and β_i for final design, $M = 0.7$, $q = 8.5$ psi.

control surfaces have a positive angle of deflection whereas the outboard have a negative value. These results are as expected when inspecting the F_n^{desired} initial and $F_n^{\text{calculated}}$ desired in Fig. 7. To "move" the $F_n^{\text{calculated}}$ initial curve toward the desired curve, the inboard portion of the curve needs to be "pulled up" (increase load, positive β_i) whereas the outboard portion of the curve needs to be "pulled down" (decrease load, negative β_i). This increase and decrease in load on the inboard and outboard portions of the wing by the control surfaces is indicated on the pressure contour plot as well.

Conclusions

Induced drag on flexible wings is reduced at off-design cruise conditions with simulated active conformal control surface deflections. The method to manipulate the spanwise distribution of load is demonstrated on two cases, a simple rectangular wing with a beam model and a fighter wing with a fully built-up finite element structural model. Conformal control surfaces are envisioned to eliminate the edge effects of conventional control surfaces, which increases profile drag. The control surfaces are deflected to redistribute the lift on the wing while maintaining a flexible trimmed (lift and pitch) flight condition. Iteratively optimizing an approximate problem eliminates the need for the trimmed angle of attack and the elevator deflections to participate in the design optimization as free variables. Only the control surface deflections are used to match the desired elliptic load distribution, which in turn is shown to produce the minimum induced drag according to calculations by a Trefftz-plane technique. The ASTROS program is used for creating a complex structural model, a realistic linear aerodynamic prediction technique, and a free flying trim analysis.

References

[1] Weisshaar, T. A., Duke, D. K., and Dobbins, A., "Induced Drag Reduction Using Aeroelastic Tailoring with Adaptive Control Surfaces," *44th AIAA SDM Conference*, AIAA Paper 2000-1619, 2000.

[2] Raveh, D. E., and Levey Y., "CFD-Based Aeroelastic Response of an Active Aeroelastic Wing," *48th AIAA SDM Conference*, AIAA Paper 2004-1515, 2004.

[3] Kuzmina, S., Ishmuratov, F., Kuzmin, V., and Sviridenko, Y., "Estimation of Flying Vehicle Induced Drag Changing Due to Deformation of Lifting Surfaces," *CEAS/AIAA International Fourm on Aeroelasticity and Structural Dynamics*, Amsterdam, 2003.

[4] Eller, D., and Heinze, S., "Approach to Induced Drag Reduction with Experimental Evaluation," *Journal of Aircraft*, Vol. 42, No. 6, Nov.–Dec. 2005, pp. 1478–1485.

[5] Neill, D. J., and Herendeen, D. L., "ASTROS User's Manual," Universal Analytics WL-TR-96-3004, Torrance, CA, May 1995.

[6] Eastep, F. E., and Olsen, J. J., "Transonic Flutter Analysis of a Rectangular Wing with Conventional Airfoil Sections," *AIAA Journal*, Vol. 18, No. 10, Oct. 1980, pp. 1159–1164.

[7] Bishop, J. A., Eastep, F. E., Striz, A. G., and Venkayya, V. B., "Influence of Model Complexity and Aeroelastic Constraints on Multidisciplinary Optimization of Wings," *Journal of Aircraft*, Vol. 35, No. 5, 1998, pp. 784–790.

[8] Sanders, B., Eastep, F., and Forster, E., "Aerodynamic and Aeroelastic Characteristics of Wings with Conformal Control Surfaces for

Morphing Aircraft," *Journal of Aircraft*, Vol. 40, No. 1, 2003, pp. 125–134.

[9] Jones, R. T., *Wing Theory*, Princeton Univ. Press, Princeton, NJ, 1990, pp. 105–111.

[10] Munk, M. M., "Minimum Induced Drag of Aerofoils," NACA Report No. 121, 1921, pp. 373–390.

[11] Ashley, H., and Landahl, M., *Aerodynamics of Wings and Bodies*, Dover, New York, 1985, pp. 135–237.

[12] Kolonay, R. M., Eastep, F. E., and Sanders, B., "Optimal Scheduling of Control Surfaces on a Flexible Wing to Reduce Induced Drag," *10th AIAA/ISSMO Multidisciplinary Analysis and Optimization Conference*, AIAA Paper 2004-4362, 2004.